JSEE Vol. 24, No. 1&2, 2022 DOI: 10.48303/jsee.2023.1998793.1053

Research Paper

Structural Analysis of the Western Part of Shotori Mountain Range; Eastern Iran

Razieh Abbaspour[1], Ahmad Rashidi[2*], Seyed Morteza Mousavi[3], Shahram Shafieibafti[4], Majid Nemati[5] and Reza Derakhshani[6]

1. Ph.D. Candidate, Department of Geology, Faculty of Earth Science, University of Birjand, Birjand, Iran
2. Associate Professor, Department of Earthquake Research, Shahid Bahonar University of Kerman, Kerman, and International Institute of Earthquake Engineering and Seismology (IIEES), Tehran, Iran, *Corresponding Author; email: rashidi@uk.ac.ir
3. Associate Professor, Department of Geology, Faculty of Earth Science, University of Birjand, Birjand, Iran
4. Associate Professor, Department of Geology, Shahid Bahonar University of Kerman, Kerman, Iran
5. Professor, Department of Geology, Shahid Bahonar University of Kerman, Kerman, Iran
6. Associate Professor, Department of Earth Sciences, Utrecht University, Utrecht, Netherlands

Received: 20/03/2023
Revised: 13/05/2023
Accepted: 13/05/2023

ABSTRACT

NW-SE trending Shotori range has some structural elements such as folds and fractures (including thrust and strike-slip faults), following almost a similar trend. Based on the plotted stereograms, the predominant mechanism of the region's faults is thrust with a dextral strike slip component which implies overcoming compressive stresses in the region. On the other hand the strike-slip horizontal component of the faults may also be due to the Nayband fault activities on Shotori and Esfandiar thrust zones. The steep dip of these faults may also be due to some normal faults converted to reverse faults as a result of stress phase change from tensional to compressional. Based on planar axis perpendicular compression or stretching axis σ_1= 34, 10 and σ_3= 296, 38 were obtained for the study area. Striogram axial surface folds dominantly show NW-SE direction, which is indicates compression axis which is equal N53, 12.Aeromagnetic data analysis revealed two magnetic lineaments with the same trends as surveyed lineaments in the field. The relatively high magnetic intensity of these lineaments could be due to basement faults in the region. With regards to obtained stereo plots, trend of the folds' axis are parallel to the regional thrust faults and folds' contour diagrams apply asymmetric folds with faulting in the area.

Keywords:
Structural analysis;
Shotori mountain range;
Fault zone;
Aeromagnetic data analysis

1. Introduction

The studied area is located between 33.37 to 33.67 N and 57.1 to 57.37 E in parts of Shotori ranges, south east of Tabas, Iran (Figure 1). Since structural elements (such as faults and folds) are essential tools to identify deformations along with their patterns in each region, precise geometric and kinematic properties of these elements should be studied. Generally, such studies depend on the appearance of the structures and their measurement in outcrop scale.

According to Berberian & Mohajer-Ashjai (1977) study of seismic movements in Iran, it is related to the movement of active faults. The tectonic movements and the mechanism of reverse faults show that the Iranian plateau is located in a pressure zone. The compressive movements resulting from the convergence of the two Arabian and Eurasian plates have caused the formation of

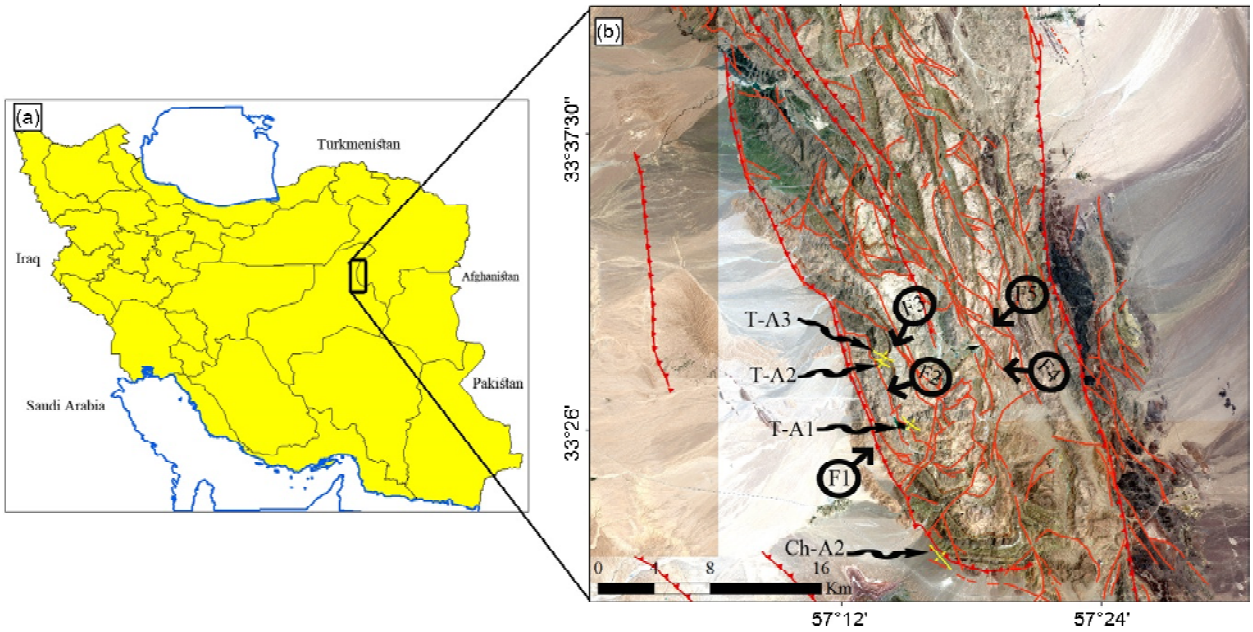

Figure 1. (a) Location of Shotori mountain range (black Rectangle) in Iran, and (b) Close-up view of the study area.

faults and folds in the northwest and southeast directions. And part of this convergence causes the activation of the Nayban and Nehbandan faults (Vernant et al., 2004; Parsons et al., 2006). Due to the location of the area in the northwest of the Lut Block and since the interaction of faults plays an important role in the deformation of the area, therefore the area is under severe stress, as a result, the intensity of fracture in this section is high and many faults have cut the rock units. Therefore, the occurred deformation process can be investigated by determining the geometric conditions of the structures. The study area is enclosed between Shotori and Esfandiar thrust zones, which includes thrust faults and folds as the most important and significant structures in the area.

In this study, each of those structures was investigated using field data, laboratory studies and satellite images. The structural model of the region was finally presented.

2. Geological Setting

Iran is located in a convergence zone between the Arabian and Eurasian plates. The convergence in Iran is primarily accommodated in the north by Alborz, in the northeast by Kopeh-Dagh, in the southwest and west by Zagros, in the east by NS strike-slip faulting, and in the southeast by Iranian Makran (Rashidi et al., 2022; Rashidi & Derakhshani, 2022; Ghanbarian & Derakhshani 2022; Saccani et al., 2022; Ezati & Gholami, 2022). GPS studies show that the deformation in Iran is heterogeneous and different blocks and faults accommodate part of this convergent deformation (Vernant et al., 2004). The progressive closure of the Neo-Tethyan ocean has led to the generating the numerous mountain ranges from the Alps to the Himalayas (Tapponnier et al., 1981; Dercourt et al., 1986). In Iran, the collision was responsible for the formation of the Zagros, Alborz, the local mountain range within the Central Iran (e.g. Shotori mountain range), and Sistan orogenic belt (Figure 1a) (e.g. Stacklin, 1968; Tirrul et al., 1983; Agard et al., 2011). Synchronous the metamorphic and crystallized rocks of the Precambrian were broken, which mostly occurred in the central regions of Iran such as the Shotori sedimentary basin.

The study indicates that the development of the young fold-thrust mountain belts necessarily involves basement shortening (thin-and thick-skinned tectonics) and that the 'frontal reverse faults' in young active fold-thrust mountain belts are the most seismically active faults. Geological and seismic data propose that the active frontal reverse fault possibly reactivated old normal faults and may add support to the contention of

reversal of fault motion during re thickening of continental crust. The active 'thin-and thick-skinned tectonics' documented in this study may prevail in other young and active fold-thrust mountain belts, which are characterized by a thick sequence of telescoped top sedimentary cover over a decollement detachment zone (Berberian, 1982).

3. Methods

In order to study and carry out this research, using geological maps and available resources, communication routes, geographical and geological conditions of the study area were investigated. A field visit was conducted in order to investigate the geological structures of the region, such as the characteristics of faults and folds. The data obtained from the field observations were processed and interpreted and analyzed using the available software, and in StereoNett, FaultKinWin, and StereoWin, after combining the field studies and the results of data interpretation and analysis, the desired structural results for area is obtained. And also, there are many folds and faults in the study area, which indicates the active tectonics of the study area.

Faults are one of the important structures in the study area, and in order to identify them, a lot of time has been spent on field surveys. Then the specifications of the faults are analyzed using related software and the mechanism of each fault is obtained.

As a result of tectonic movements (orogeny), layered rocks have a different shape, and as a result of this process, smooth surfaces become curved surfaces, and these curved surfaces are called folds. By using the folds, it is possible to determine the deformation history of the region, because the layers were formed horizontally in the sedimentary basin from the beginning, and vertical changes have been recorded in these layers, therefore, periods of calm or tectonic intensification in the fold layers. Corrosion can be traced, and also with the continuation of deformation processes, increase in folding intensity and thickness changes in the hinge and edge of folds, the evolutionary course of deformation can be followed.

4. Discussion and Results

The structural elements that exist in an area are considered necessary and required tools for recognizing deformations and achieving a deformation pattern in that area. In order to achieve such a goal, the exact geometrical and kinetic characteristics of those structures should be studied. Faults and folds are among the structures in the study area that can be used to determine the deformation pattern of the region. The area under study is a folded and discrete area that has been affected by tectonic movements, many folds and faults have been created in it. Pliocene orogenic activities have played a role in the formation of the young face of Shetri Mountains. Based on plotted stereograms, the dominant mechanism of the faults is strike-slip with dextral component, which indicates the dominance of compressional stresses in the region. On the other hand, the high dip of these faults can be indicative of normal faults, which act as reverse after the late Triassic tensile to compressional stress phase changes.

Aeromagnetic maps (resulted after applying Reduction to Pol and upward continuation filters) show two magnetic lineaments with compatible orientation to surveyed lineaments in the region. Relatively high magnetic intensity of these lineaments can be due to their basement origin or existence of basement faults in the area.

For the perpendicular method, the compressional and minimum stress axis were obtained as σ_1 = 34,10 and σ_3 = 269,38 respectively, in the study area. These results are compatible with the model obtained by Research Center of Seismology with determined horizontal component of compressional axis and maximum force for the study area.

Contour diagrams of the axial planes' pole show the prevailing Northeast-Southwest trend that is the N53,12 Z axis, having a very good compatibility with the dominant stress obtained by the faults (σ_1 = 34,10) and implies the existence of asymmetric folds within the fault.

Aeromagnetic data interpretation revealed an increase in intensity of the magnetic field from west to east of the mountains which can be due to igneous rocks and increase in depth of basement faults in the region.

Based on laboratory modeling results, folds of the region are exotic, asymmetric with thrust faults having nearly horizontal slopes in depth and vertical near the surface and showing their folding effects.

Since the study area is surrounded by Shotori (West) and Esfandiar (East) thrust zones and also due to the stress field in the region, geological formations (such as Jamal, Sorkh shale and Shotori) have undergone folding and deformations. Hence, in order to determine the deformation pattern and structural mountain range of the region, structural elements (faults and folds) were studied in detail. Accordingly, faults and folds of the western part of Shotori mountain range were studied during some surveys. Perpendicular method was used for Geometric-Kinematic analysis of the faults while Fourier analysis, inter-limb angle, geological orientation and Ramsay & Huber (1987) and Fluety (1964) classifications were used for analysis of the folds. Shape of the curves can be determined with Fourier analysis using trigonometric functions series. Fourier analysis with coordination of fold shape harmonic was first proposed by Stabler (1968) and developed by Huddleston (1973) afterwards. He classified a section of the whole folded planes using only two Fourier coefficients, b1 and b3, and finally specified six standard shapes of type A (Box folds) to Type F (Chevron folds) and five standard swing amplitude.

Fluety (1964) Classification is based on the position of axial plane first and then hinge line (fold hinge plunge).

The other classification is based on interlimb angle. In this method, declining the angle between the limbs reflects higher degree of folding. Accordingly, folds were classified into six groups as tabulated in Table (1).

Turner & Weiss (1963) classified nearly plane cylindrical folds based on the geological orientation of the hinge line and axial plane (Table 2).

Ramsey classification considers the curvature of folded surface and changes in fold thickness. It is the best classification method presented for folds as it is based on Dip isogon line.

4.1. Geological Evidence

Geological evidence includes those movements and deformations that began at the end of the Tertiary and continue until now. Among these movements and deformations that occurred in the region, we can mention thickening, faulting, folding and young fractures in rock units. In the following, we have described some of these deformations.

4.1.1. Faults in the Study Area

4.1.1.1. Fault F1

This fault is a branch of Shotori thrust in the border between mountains and plains. Geometric position of the fault's plane is 57°13'38"E and 33°25'45"N, N340°/85°NE and rake is 60° north.

Table 1. Different types of folds based on Interlimb angle.

Fold Type	Interlimb Angle
Gentle Fold	120-180
Open Fold	70-120
Close Fold	30-70
Tingle Fold	0-30
Isoclinal Fold	0
Fan Fold	-

Table 2. Fold classification based on orientation of the geologic orientation and axial plane.

	Orientation of Hinge Line			
		Horizontal	Plunging	Vertical
Axial Plane Orientation	Vertical	Horizontal Normal Fold	Normal Inclined Fold	Vertical
	Inclined	Inclined Horizontal Fold	Inclined Plunging Fold	
			Inclined Fold	
	Horizontal	Recumbent		

Based on the plotted stereogram, the fault mechanism is reverse with a dextral strike-slip component (Figure 2).

4.1.1.2. Fault F2

Fault plane is located on 57°14'57"N, 33°26'30"E with N115°/87°NE with slickenlines which rake 60° northward. Plotted stereogram shows a vertical fault with a strike-slip component (Figure 3).

4.1.1.3. Fault F3

Fault plane is located at 57°15'5"N, 33°26'56"E with N170°/40°NE with slickenlines, which rake 20° northward. Plotted stereogram shows the reverse mechanism of the fault with dextral strike-slip component (Figure 4).

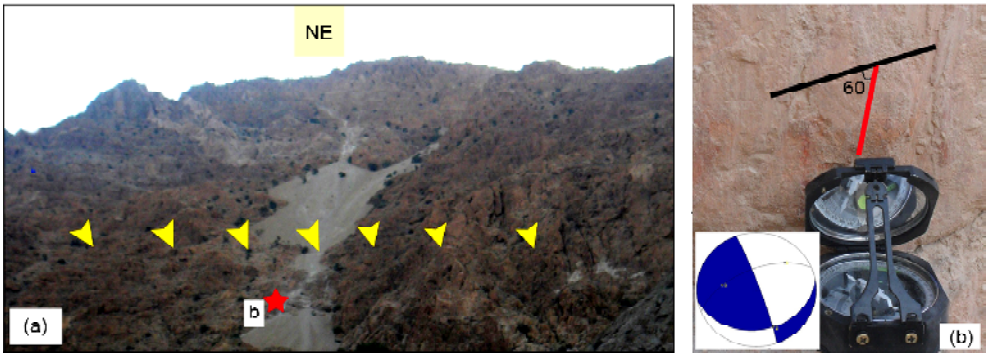

Figure 2. Outcrop of the F1 fault. a) Fault near Zerk village. Fault surface trace is specified by yellow arrows, location fault plane (red star). (b) A view of slicken lines on the fault plane, with fault related stereograms.

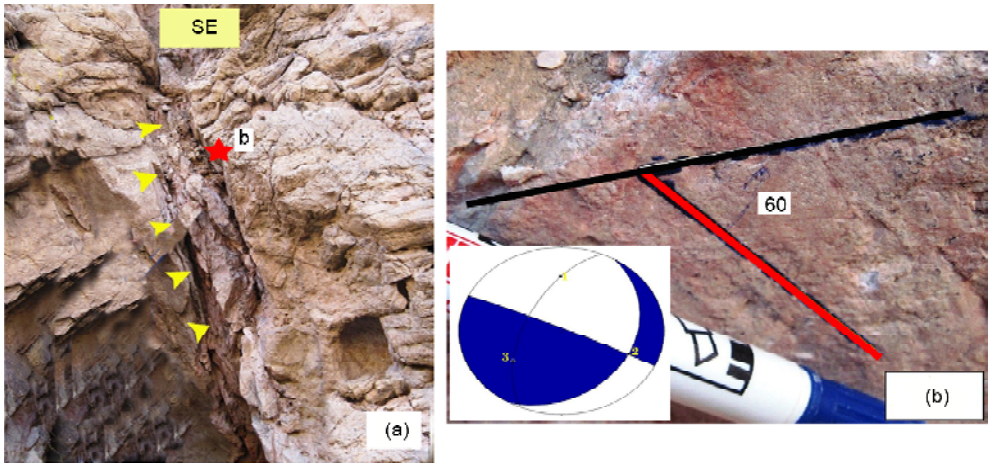

Figure 3. Outcrop of the fault F_2 (view to the South East). (b) A close-up view of slickenline on the fault plane with stereograms of the fault plane.

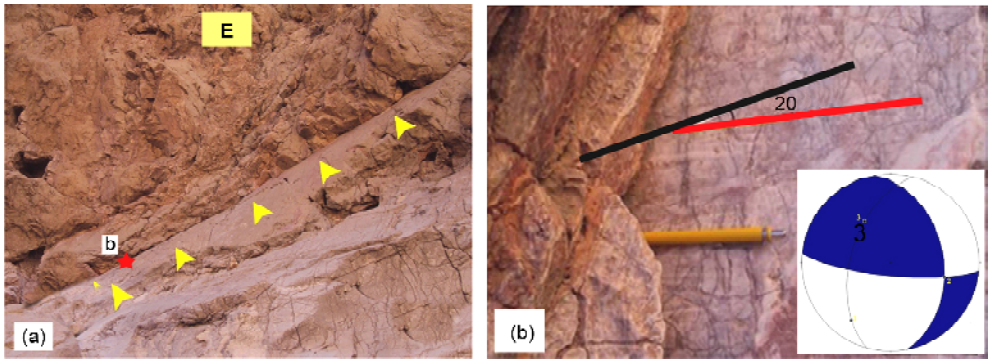

Figure 4. (a) Outcrop of the fault F_3, View to the southeast (b) A close-up view of slicken lines on the fault plane, and stereogram of the related fault.

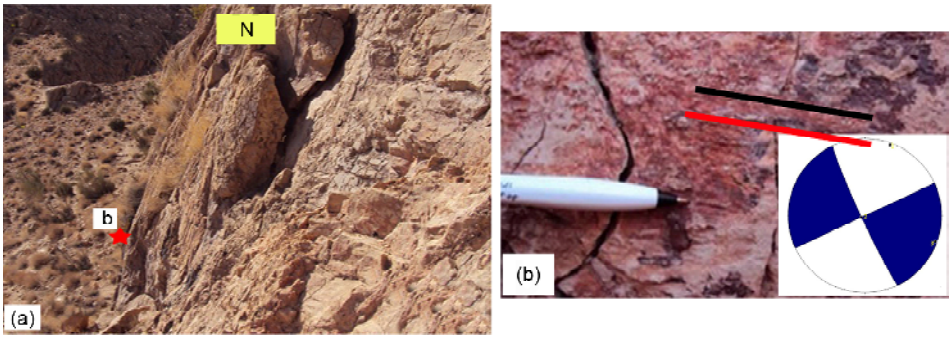

Figure 5. (a) Outcrop of the fault F4.(b) A view of slickenlines on the fault plane, and Stereograms and stress axis of the related fault.

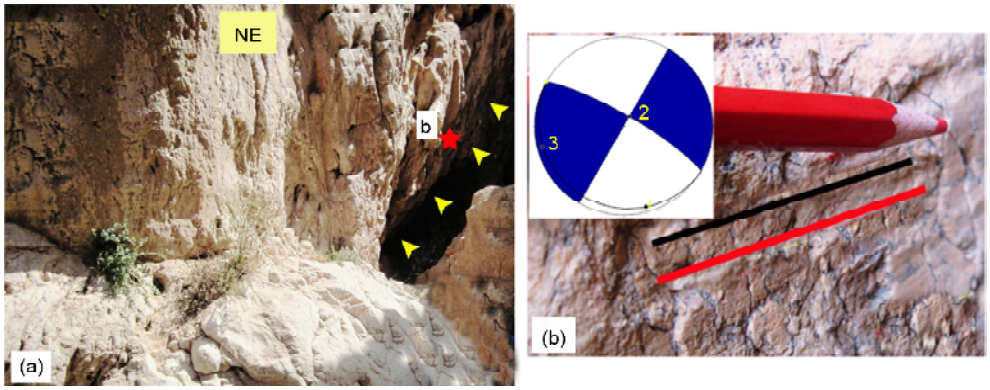

Figure 6. (a) Outcrop of the fault F5., (b) A close-up view of scratch lines on the fault plane, with Stereograms and of the fault.

4.1.1.4. Fault F4

The fault plane is located at 57°19'19"N and 33°27'15"E, N335°/85°SW with Slickenlines which rake 0°. According to stereograms, the fault mechanism is dextral strike-slip. As shown in Figure (5), the height difference between height of hanging wall and the footwall of the fault is high.

4.1.1.5. Fault F5

This fault is located at 57°18'25"N, 33°29'18"E, N300°/80°NE with slickenlines, which rake 0° in the Sorond village. Fault scarp of F5 is 22 m high.

Slickenlines on the fault's plane indicate a dextral movement. As shown in Figure (6), the stereogram relating to the fault shows a dextral strike-slip mechanism. Sorond spring, one of the main springs of the village, is a result of this fault.

The dominant mechanism of the faults in the region is reverse with dextral strike-slip component, which indicates the conquest of compressive stresses in the region. On the other hand, the horizontal strike-slip component of those faults can also be due to the Nayband fault activities on Shotori and Esfandiar thrust zones. Based on Dihedral method, the maximum and minimum stress axis in the studied region were obtained as 34/10 and 296/38 respectively, (σ_1 = 34,10, σ_3 = 296,38).

4.1.2. Folds of the Region

4.1.2.1. Fold CH (Chirouk) -A2

This fold is located on the way from Chiruk to Kurite dam in Jamal limestone. It is a very high intensity fold located on N 290 / 34 axis. It was surveyed at 57°15'12"N, 33° 22'48"E (Figure 7).

Parameters measured in CH-A1 fold are provided in (Table 3).

4.1.2.2. Fold T (Tangale Modar) -A1

This anticline with N 148/08 axis is exposed at the beginning of Tangal-e Maudar and in Shotori formation. Location of the survey point is 57°12'02" N, 33°26'22"E (Figure 8).

Parameters measured in fold T-A1 are provided in (Table 4).

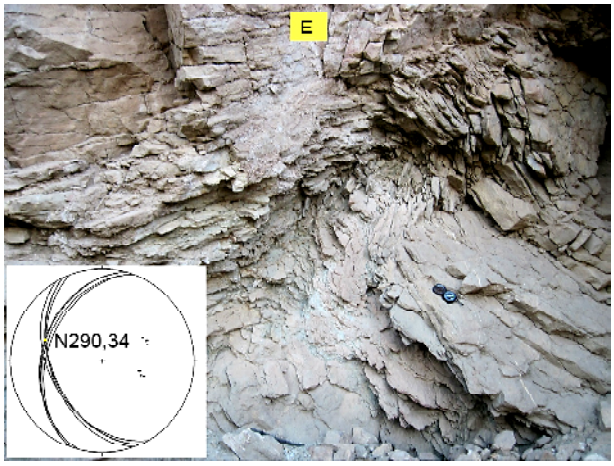

Figure 7. A view of CH-A2 fold, view to the east, with Stereoplot related to fold limbs and axis.

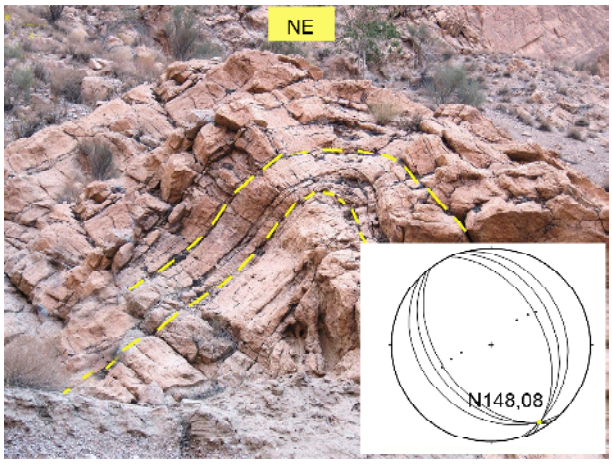

Figure 8. A view of T-A1 fold, View to the north east, and Stereoplot related to the fold limbs and axis.

Table 3. Parameters measured in fold CH-A2 and identifying it based on these parameters.

	Types of Classification	Classification Based on	Specifications of Fold	Fold Type
CH-A_2	Flutey	Interlimb Angle	150	Gentle Fold
	Geological Orientation	Axial Plane Orientation	N276/81NE	Inclined Plunging
		Hinge Line Orientation	N290/34	
	Ramsey	Thickness of Hinge and Limb (cm)	$t_a = 5.46$ $t_0 = 5.46$	1B
	Fourier Analysis	The Fourier Coefficients	$b_1 = 0.87$ $b_3 = -0.01$	Sinusoidal-Near to Chevron
	Flutey	Axial Plane's Dip	81	Moderately Plunging
		Plunge of Fold Axis	34	

Table 4. Parameters measured in T-A1 fold and identification based on these parameters.

	Types of Classification	Classification Based on	Specifications of Fold	Fold Type
CH-A_1	Flutey	Interlimb Angle	85	Open Fold
	Geological Orientation	Axial Plane's Orientation	N330/83NE	Normal Inclined Fold
		Take Sides Hinge Line	N148/08	
	Ramsey	Thickness Hinge and Limb (cm)	$t_a = 1.4$ $t_0 = 1$	1B
	Fourier Analysis	The Fourier Coefficients	$b_1 = 1$ $b_3 = -0.3$	Box Fold
	Flutey	Deep Axial Surface	83	Horizontal
		Plunge Fold Axis	08	

4.1.2.3. Fold T-A2

This anticline with N320/09 axis was surveyed in Shotori formation at 57°14'58"N, 33°26'30"E (Figure 9). Parameters measured in fold T-A2 are provided in (Table 5).

4.1.2.4. Fold T-A3

This is an anticline with N354/20 axis and has an outcrop at 57°14'57"N, 33°26'30"E in Shotori formation (Figure 10).

Based on stereoplots of the fold limbs, the fold axis trend of the studied area is NW-SE, parallel to the faults of the region and Shotori Mountains. Also, considering the contour diagram of their limb's pole, most folds in the region are of asymmetric type. Parameters measured in fold T-A3 are provided in (Table 6).

4.2. Identifying Magnetic Lineaments

Aeromagnetic data play a unique role in studying

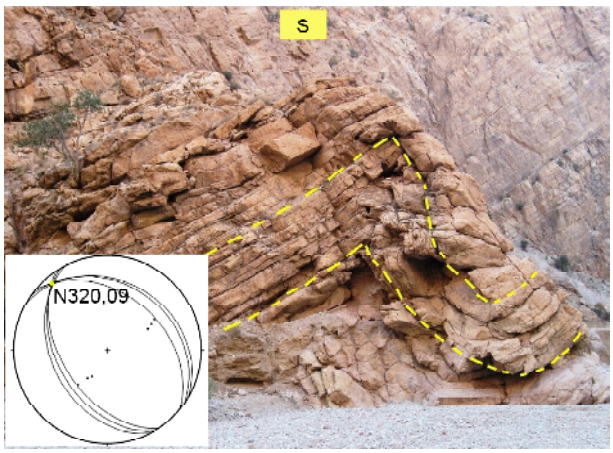

Figure 9. T-A2 fold, view to the south., and stereoplots of the fold limbs and axis.

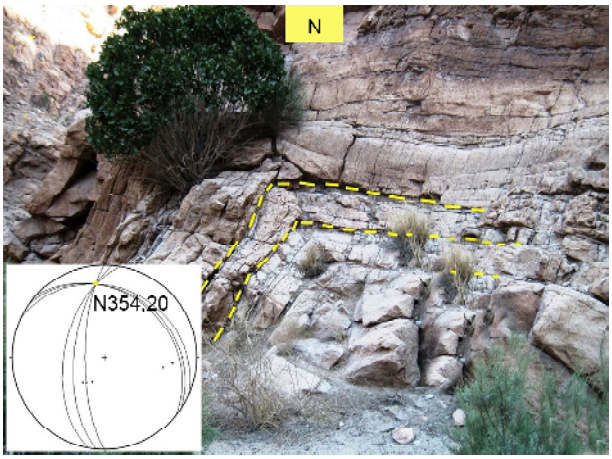

Figure 10. A view of T-A3 fold, view to the north, with stereoplot related to the fold limbs and axis.

Table 5. Parameters measured in T-A2 fold and identification based on these parameters.

	Types of Classification	Classification Based on	Specifications of Fold	Fold Type
T-A2	Flutey	Interlimb Angle	73	Open Fold
	Geological Navigation	Take Sides Plane Axial	N322/86NE	Inclined Fold
		Take Sides Hinge Line	N320/09	
	Ramsey	Thickness Hinge and Limb (cm)	ta = 47.35 t0 = 47.35	1B
	Fourier Analysis	The Fourier Coefficients	b1 = 1.14 b3 = - 0.02	Chevron-Sine Wave
	Flutey	Deep Axial Surface	86	Horizontal
		Plung Fold Axis	09	

Table 6. Parameters measured in T-A3 fold and identification based on these parameters.

	Types of Classification	Classification Based on	Specifications of Fold	Fold Type
T-A3	Flutey	Interlimb Angle	75	Open Fold
	Geological Navigation	Axial Plain Orientation	N346/73NE	Inclined Fold
		Hinge Line Orientation	N354/20	
	Ramsey	Thickness of Hinge and Limb (cm)	ta = 77.20 t0 = 87.50	3
	Fourier Analysis	The Fourier Coefficients	b1 =3.15 b3 = 1.02	Near Chevron
	Flutey	Axial Surface Dip	73	Inclined Plunging
		Fold Axis Plunge	20	

processes occurring in geological units by means of tracking changes in the magnetic field. Location and depth of the shear zones, fractures in basement, identifying hidden plutons, investigating tectonic condition of areas and study of their relationship with magmatic masses and mineralization are some of the identifiable factors using aeromagnetic data (Robinson & Coruh, 1988).

Aerial magnetism data have been used along straight lines that are usually in line with the structures of aerial magnetism data that were taken with a flight line distance of 7.5 km and by a helicopter at an average flight height of 60 meters above the ground. In general, due to the presence of many disturbing factors and the large volume of collected data, it is necessary to make various corrections on the data (Dobrin & Savit, 1988). By applying different filters of reduction to pole (Reduction to Pole) and continuation beyond (Downward Continuation) on the data of total magnetic intensity (TMA) of the region (Figure 11), they can be examined from different aspects and

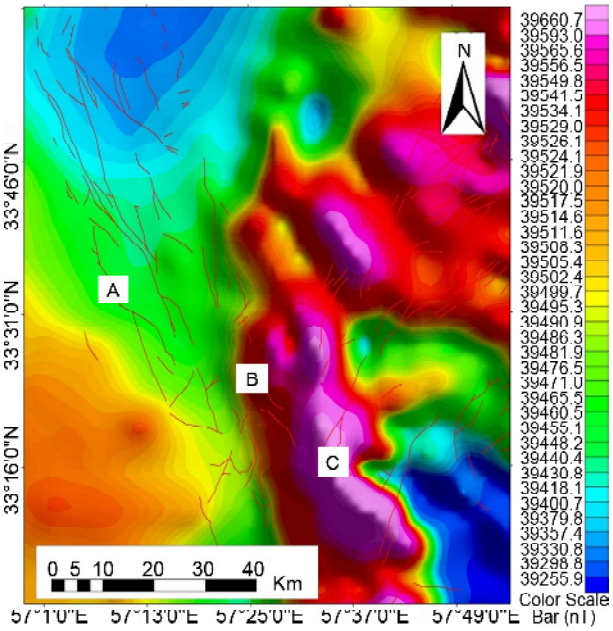

Figure 11. Total Magnetic Anomaly (TMA).

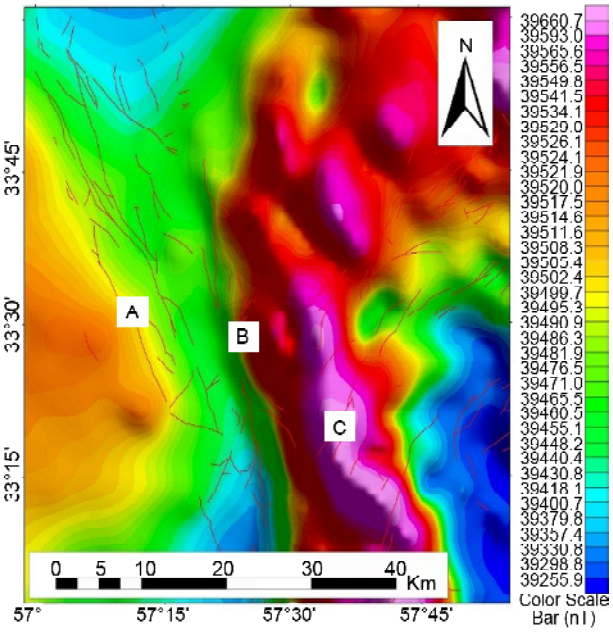

Figure 12. Reduction to Pole map of the study area.

then by combining this information with geological data, the final analysis and interpretation can be extracted from them.

4.2.1. Reduction to Pole

By using this filter, the magnetic field is transferred from a magnetic latitude where the vector of the earth's field is slanted to the magnetic pole, that is, where the induced field is vertical, because if the earth's field is slanted, the shape of the magnetic anomalies that are Inductions have arisen; it will be asymmetric with respect to the generating sources, but if the induced field is vertical, the anomalies caused by magnetic induction will be placed on their source. Therefore, the interpretation of aerial magnetism data is usually done on the different image of the pole, and on this basis, it leads to a more appropriate diagnosis of masses. By comparing the map resulting from this filter with the map of the entire magnetic field, a shift towards the northwest is observed in the anomalies (Figure 12). By applying this filter and the map resulting from this filter, it is possible to consider the possibility of a magnetic line in the A, B, and C ranges due to the large change in the amount of anomaly (Figure 12).

4.2.2. Upward Continuation

By applying the transversal filter, by which the magnetic field data from a base surface is mathematically imaged on a level surface above the main base, it has been used to make the effect of masses and deeper faults more visible. The maps obtained from this filter (at higher levels of 500 and 1000 meters) show that the origin of anomalies in the region is deep or severe (Figure 13).

Resulting maps of this filter (at levels of 500 and 1000 m) indicate that the origin of anomalies in the area is deep or intensive (Figure 12). Accordingly, sharp borders with sharp gradients in high level maps represent the basement origin of faults, especially NW-SE orientation ones (A and B regions).

Magnetic lineaments identified by applied filters on the aeromagnetic data, are in agreement with the information obtained from field data and satellite images. Thus, the important structural NW-SE trends in magnetic data act is profound and basic.

A high magnetic strip (purple) in the eastern part of the mountain ranges is related to the volcanic masses. Dense contours in the eastern and western parts of the mountains show the high intensity of the magnetic field, which could be due to the deep basement. The most important reasons, because the mechanisms are reverse faults in the area and may become deep, slope close to the horizon and a Listric state have been

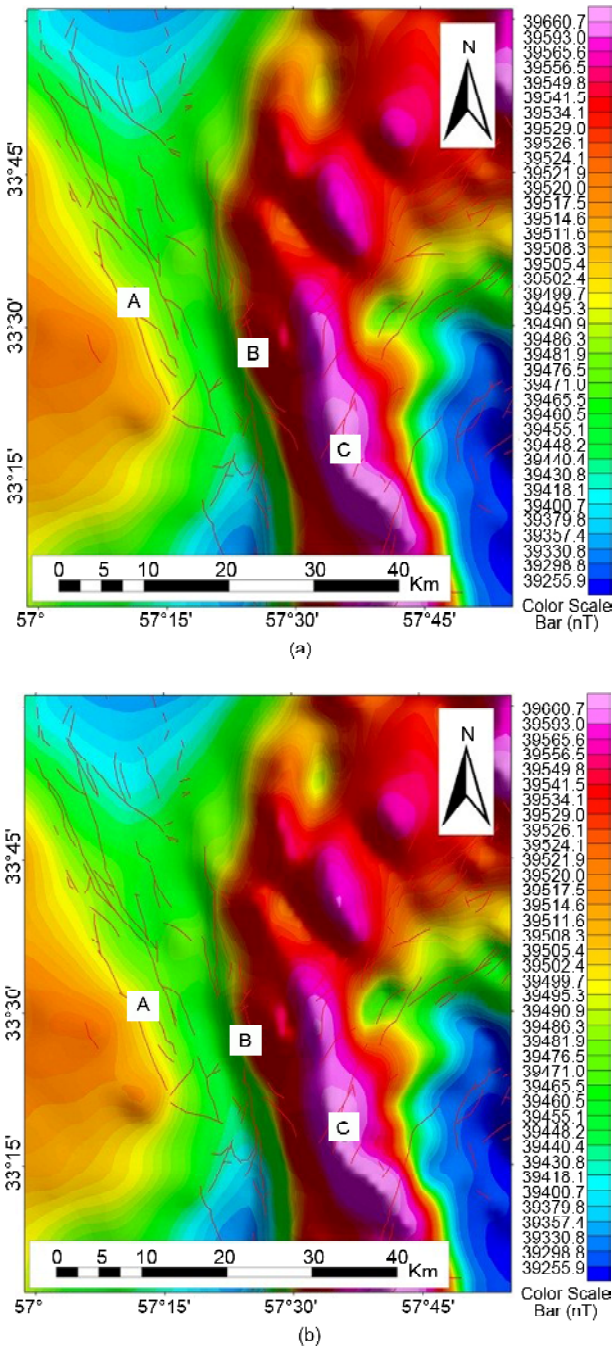

Figure 13. (a) Upward continuation map of the study area (500 m), (b) Downward continuation map of the study area (1000 m).

found to appear. The intensity of the magnetic field increased from west to east along with increasing slope of the NW-SE trending lineaments. This could be an indication of basement faults which are deeper to the east thereby causing the eruption of igneous.

4. Conclusions

Based on the plotted stereograms, the predominant mechanism of the region's faults is thrust with a dextral strike slip component which implies overcoming compressive stresses in the region. The steep dip of these faults may also be due to some normal faults converted to reverse faults as a result of stress phase change from tensional to compressional. With regards to obtained stereo plots, trend of the folds' axis are parallel to the regional thrust faults and folds' contour diagrams apply asymmetric folds with faulting in the area.

According to the perpendicular dihedral method, the perpendicular axis of the pressure, i.e., $\sigma = 34.10°$ and the tension axis $\sigma_3 = 296.38$, was obtained for the study area. This model is consistent with the model that the Earthquake Group and the Seismological Research Institute have determined the horizontal component of the pressure axis and the maximum force for the study area.

Aerial geomagnetic data (types of filters such as Reduction to Pole, Upward continuation) show two magnetic lines, the alignment of these lines is consistent with the lines taken in the field operations. The almost high magnetic intensity in these lines can be due to the presence of bedrock faults in the region.

References

Agard, P., Omrani, J., Jolivet, L., Whitechurch, H., Vrielynck, B., Spakman, W., ... & Wortel, R. (2011). Zagros orogeny: a subduction-dominated process. *Geological Magazine*, *148*(5-6), 692-725.

Berberian, M. (1982). Aftershock tectonics of the 1978 Tabas-e-Golshan (Iran) earthquake sequence: a documented active thin- and thick-skinned tectonic case. *Geophys. J. R. Astr. Soc.*, *68*, 499-530.

Berberian, M., & Mohajer-Ashjai, A. (1977). Seismic risk map of Iran, a proposal. *Geol. Surv. Iran*, *40*, 121-148.

Dercourt, J., et al. (1986). Geological evolution of the Tethys belt from the Atlantic to the Pamirs since the Lias. *Tectonophysics*, *123*(1), 241-315.

Dobrin, M.B., & Savit, C.H. (1988). *Introduction to Geophysical Prospecting* (4th edn). McGraw Hill, New York.

Ezati, M., & Gholami, E. (2022). Neotectonics of the Central Kopeh Dagh drainage basins, NE Iran.

Arab. J. Geosci., *15*, 992.

Fluety, M.J. (1964). The description of folds. *Proceedings of the Geologist Association*, 75p., 461-492.

Ghanbarian, M.A., & Derakhshani, R. (2022). The folds and faults kinematic association in Zagros. *Scientific Reports*, *12*(1), 8350.

Huddleston, P.J. (1973). Fold morphology and some geometrical implications of theories of fold development. *Tectonophysics*, *16*, 1-46.

Parsons, B., Wright, T., Rowe, P., Andrews, J., Jackson, J., Walker, R., ... & Engdahl, E. R. (2006). The 1994 Sefidabeh (eastern Iran) earthquakes revisited: new evidence from satellite radar interferometry and carbonate dating about the growth of an active fold above a blind thrust fault. *Geophysical Journal International*, *164*(1), 202-217.

Rahimi Chakdel, A., & Nabavi, T. (2013). *Structural Geology*. Golestan University Press, 416p.

Ramsay, J.G., & Huber, M. (1987). *The Techniques of Modern Structural Geology, V.2: Folds and Fractures*. Academic Press, London, *391*, 309-700.

Rashidi, A., & Derakhshani, R. (2022). Strain and moment rates from GPS and seismological data in northern Iran: implications for an evaluation of stress trajectories and probabilistic fault rupture hazard. *Remote Sensing*, *14*(9), 2219.

Rashidi, A., Khatib, M.M., & Derakhshani, R. (2022). Structural characteristics and formation mechanism of the earth fissures as a geohazard in Birjand, Iran. *Applied Sciences*, *12*(9), 4144.

Robinson, E.S., & Coruh, C. (1988). *Basic Exploration Geophysics*. Wiley, New York.

Saccani, E., Delavari, M., Dolati, A., Pandolfi, L., Barbero, E., Brombin, V., & Marroni, M. (2022). Geochemistry of volcanic rocks and dykes from the Remeshk-Mokhtarabad and Fannuj-Maskutan Ophiolites (Makran Accretionary Prism, SE Iran): New constraints for magma generation in the Middle East Neo-Tethys. *Geosystems and Geoenvironment*, 100140.

Stabler, C.L. (1968). Simplified Fourier analysis of fold shapes. *Tectonophysics*, *6*(4), 343-350.

Stocklin, J. (1968), Structural history and tectonics of Iran: A review. *Am. Assoc. Pet. Geol. Bull.*, *52*(7), 1229-1258.

Stockline, J., Eftekhar-Nezad, J., & Hushmand-zadeh, A. (1965). Geology of the Shotori Range (Tabas area, East Iran). *Geol. Surv. Iran,* 3.

Tapponnier, P., et al. (1981). The Tibetan side of the India-Eurasia collision. *Nature*, *294*(5840), 405-410, doi:10.1038/294405a0.

Tirrul, R., Bell, I.R., Griffis, R.J., & Camp, V.E. (1983). The Sistan suture zone of eastern Iran. *Geological Society of America Bulletin*, *94*(1), 134-150.

Turner, F. J., and Weiss, L. E.(1963). *Structural Analysis of Metamorphic Tectonites*. New York: McGraw-Hill, 545p.

Vernant, P., Nilforoushan, F., Hatzfeld, D., Abbassi, M. R., Vigny, C., Masson, F., ... & Chéry, J. (2004). Present-day crustal deformation and plate kinematics in the Middle East constrained by GPS measurements in Iran and northern Oman. *Geophysical Journal International*, 157(1), 381-398.